Dalton Transactions

ROYAL SOCIETY OF CHEMISTRY

COMMUNICATION

View Article Online
View Journal | View Issue

Cite this: *Dalton Trans.*, 2021, **50**, 5437

Received 17th March 2021,
Accepted 12th April 2021

DOI: 10.1039/d1dt00878a

rsc.li/dalton

Enhancing the chemical flexibility of hybrid perovskites by introducing divalent ligands†

Lydia G. Burley,[a] James H. Beecham-Lonsdale,[a] Anant Kumar Srivastava,[a,b] Ines E. Collings[c] and Paul J. Saines*[a]

Herein we report the synthesis and structures of $[(CH_3)_2NH_2]Er(HCO_2)_2(C_2O_4)$ and $[(NH_2)_3C]Er(HCO_2)_2(C_2O_4)$, in which the inclusion of divalent oxalate ligands allows for the exclusive incorporation of A^+ and B^{3+} cations in an ABX_3 hybrid perovskite structure for the first time. We rationalise the observed thermal expansion of these materials, including negative thermal expansion, and find evidence for weak antiferromagnetic coupling in $[(CH_3)_2NH_2]Er(HCO_2)_2(C_2O_4)$.

Perovskites have long dominated the field of functional materials due to the wide range of conducting, ferroelectric, magnetic and catalytic properties they are known to exhibit.[1–5] This is largely due to the high degree of chemical flexibility they can exhibit within their general ABX_3 formula (where A and B are larger and smaller cations, respectively, and X is the anionic ligand). While the focus on perovskites has traditionally been on purely inorganic materials, *e.g.* metal oxides, recently there has been tremendous interest in perovskite materials that combine both inorganic and organic building blocks. This is best known in semi-conducting phases such as $(CH_3NH_3)PbI_3$, which promise to be the next generation photovoltaics,[6–8] and $AM(HCO_2)_3$ (where A is a molecular cation and M a divalent transition metal or alkaline earth) phases where hydrogen bond driven ordering of the organic A-site cations leads to ferroelectric properties, which when combined with magnetically ordered frameworks can give rise to multiferroicity.[9–12] Such hybrid perovskites have shown tremendous chemical flexibility with regards to the wide range of molecular building blocks they can incorporate on either their A-sites, where many amine related moieties have been incorporated, or X-site, where monovalent ligands including halides, formate, hypophosphite, azide, cyanide and tetrahydroborate have been featured.[9,12–16] Inorganic–organic perovskites, however, remain much less chemically flexible than purely inorganic perovskites with regards to the range of different charges on cations they can accommodate due to the almost complete dominance of monovalent ligands in hybrid perovskites. This restricts the vast majority of "simple" ABX_3 inorganic–organic perovskites to monovalent A-site and divalent B-site cations, restricted by the total formal charge of 3^- on the ligands in their formula unit. This contrasts sharply with simple perovskite oxides where the total of 6^- on the O^{2-} ligands allows a far greater range of cation charges to be incorporated, with A^+/B^{5+}, A^{2+}/B^{4+} and A^{3+}/B^{3+} combinations all common.[5]

The dominance of monovalent ligands in inorganic–organic ABX_3 perovskites restricts examples with B^{3+} cations to cases with either neutral A-site species, which may lead to reduced stability and less well defined stoichiometry as they are not essential for charge balance,[17–19] or a mixture of monovalent and trivalent B-site cations.[9,12] $ALn^{3+}(HCO_2)_4$ (where Ln = a lanthanide or yttrium) phases are known but this deviates from the ideal ABX_3 stoichiometry and, furthermore, in most perovskite-like $ALn^{3+}(HCO_2)_4$ phases the fourth ligand leads to additional diagonal connectivity between Ln cations increasing the number of lanthanides they are connected to from six to eight deviating from perovskite connectivity.[20–22] Realising inorganic–organic perovskites with divalent ligands has the potential to greatly enhance their chemical flexibility in a similar fashion as seen when comparing purely inorganic halide and oxide perovskites.[5] To the best of our knowledge the only hybrid perovskites with divalent ligands reported thus far are the fascinating $A^+(B^+_3B^{2+})(C_2O_4)_3$ perovzolates; their chemical flexibility is, however, much reduced compared to even other inorganic–organic perovskites.[23–25] This can be best understood by expressing their stoichiometry as

[a]*School of Physical Sciences, University of Kent, Canterbury, Kent, CT2 7NH, UK. E-mail: P.Saines@kent.ac.uk*
[b]*Department of Materials Engineering, Indian Institute of Science (IISc), Bangalore-560012, Karnataka, India*
[c]*Centre for X-ray Analytics, Empa – Swiss Federal Laboratories for Materials Science and Technology, 8600 Dübendorf, Switzerland*

† Electronic supplementary information (ESI) available: Synthetic and analytical methods, crystallographic details and CIFs from single crystal X-ray structure determination (also deposited in the CSD at entries 2068774–2068779) and figures of powder X-ray diffraction, thermal analysis, infrared spectra and magnetic property measurements. CCDC 2068774–2068779. For ESI and crystallographic data in CIF or other electronic format see DOI: 10.1039/d1dt00878a

$A^{+}_{0.25}(B^{+}_{0.75}B^{2+}_{0.25})(C_{0.5}O)_3$, highlighting that the total charge on their effective 3 X anions is a total of 1.5^{-}, coupled with a limitation to small A-site cations.

Inspired by the $ALn(HCO_2)_4$ and $A^{+}_{0.25}(B^{+}_{0.75}B^{2+}_{0.25})(C_{0.5}O)_3$ phases, in this work we have sought to explore new $AEr(HCO_2)_2(C_2O_4)$ phases in which the inclusion of the divalent oxalate ligand in place of a monovalent formate allows the inclusion of a combination of exclusively A^{+} and B^{3+} cations in a ABX_3 hybrid perovskite for the first time; Er^{3+} being the smallest economical lanthanide. Herein we report the solvothermal synthesis of $[(CH_3)_2NH_2]Er(HCO_2)_2(C_2O_4)$ and $[(NH_2)_3C]Er(HCO_2)_2(C_2O_4)$ and their crystal structures, in which the bidentate oxalate ligands lead to eight coordinate Er^{3+} cations linked to six neighbouring Er cations by a mixture of formate and oxalate linkers. We find that the A-site cation in both compounds remain ordered to at least 500 K, suggesting related phases are likely to be potential ambient temperature ferroelectrics while $[(CH_3)_2NH_2]Er(HCO_2)_2(C_2O_4)$ is weakly antiferromagnetic. We also report the anisotropic thermal expansion of these phases, rationalising negative thermal expansion (NTE) due to a framework hinging mechanism.

The two compounds reported in this work, $[(CH_3)_2NH_2]Er(HCO_2)_2(C_2O_4)$ and $[(NH_2)_3C]Er(HCO_2)_2(C_2O_4)$, were both made by solvothermal synthesis by reacting $Er(NO_3)_3{\cdot}5H_2O$, oxalic acid, sodium carbonate and either an ethanolic solution in dimethylamine or guanidinium carbonate in a 1 : 1 mixture of deionised water : *N*,*N*-dimethlyformamide at 100 °C (see ESI† for further details). $[(CH_3)_2NH_2]Er(HCO_2)_2(C_2O_4)$ is *P*2/*n* monoclinic while $[(NH_2)_3C]Er(HCO_2)_2(C_2O_4)$ adopts *Pcca* orthorhombic symmetry, space group numbers 13 and 54, respectively (see Fig. S1 and S2† for depictions of the asymmetric units). The differences in symmetry likely arises from the shape and orientation of the molecular cations given the similarity of other aspects of the structure. Each Er^{3+} cation is coordinated to one oxygen from each of the two carboxylates in two oxalate linkers and four oxygen atoms from different formate linkers. This leads to all Er^{3+} cations being eight coordinate in a square antiprismatic geometry (see Tables S2 and S3† for selected coordination bond distances and angles), a significant departure from the octahedral B-site cations of conventional perovskites enabled by the bidentate oxalate ligand. Crucially, however, the compound can be viewed as adopting a hybrid perovskite structure since the bidentate oxalate ligand is acting as a single linker between neighbouring polyhedra leading to each ErO_8 polyhedra being connected to only the expected six neighbours (see Fig. 1 for depiction). Herein we will therefore refer to these compounds as hybrid perovskites, retaining the phrase perovskite-like for structures that deviate from perovskite connectivity and/or ABX_3 composition, *e.g.* related layered structures, those with ordered B-site cation vacancies or the aforementioned $ALn(HCO_3)_4$ phases.

In $[(CH_3)_2NH_2]Er(HCO_2)_2(C_2O_4)$, the oxalate ligands provide connectivity along both directions in the *ab* plane, alternating with formate linkers, while the other distinct formate linkers provide connectivity along the *c*-axis. Similar connectivity also occurs in $[(NH_2)_3C]Er(HCO_2)_2(C_2O_4)$ but in this case the

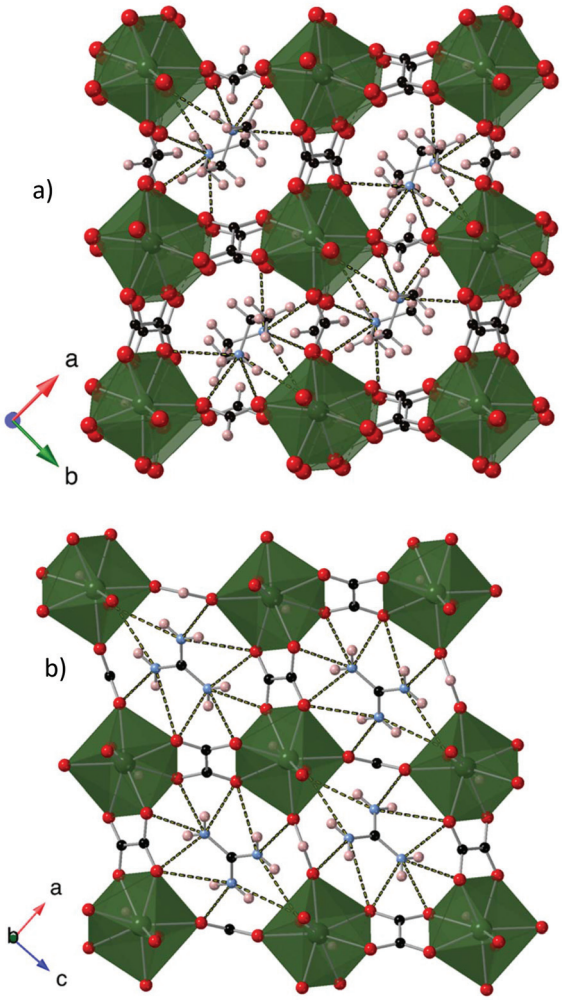

Fig. 1 Crystal structures of (a) $[(CH_3)_2NH_2]Er(HCO_2)_2(C_2O_4)$ and (b) $[(NH_2)_3C]Er(HCO_2)_2(C_2O_4)$. ErO_8 polyhedra are shown in dark green while carbon, oxygen, nitrogen and hydrogen atoms are shown in black, red, blue and pink, respectively. Hydrogen bonds are shown between donor and acceptor atoms as yellow dotted lines.

formate linkers provide connectivity along the *b*-axis and alternate with oxalates in the *ac* plane. All Er cations have bond valence sums consistent with Er^{3+}, with the two distinct cations in $[(CH_3)_2NH_2]Er(HCO_2)_2(C_2O_4)$ being 2.99 and 3.01 while in $[(NH_2)_3C]Er(HCO_2)_2(C_2O_4)$ they are 3.06, using structures determined at 293 and 310 K, repectively.[26]

The unit cells of $[(CH_3)_2NH_2]Er(HCO_2)_2(C_2O_4)$ and $[(NH_2)_3C]Er(HCO_2)_2(C_2O_4)$ are $\sqrt{2} \times \sqrt{2} \times 2$ and $\sqrt{2} \times 1 \times 2\sqrt{2}$ supercells of an undistorted (and unrealised) parent phase (see Fig. S3 & S4† for full depiction of units cells). In $[(CH_3)_2NH_2]Er(HCO_2)_2(C_2O_4)$ this appears to result from the alternating orientation of the equivalent $[(CH_3)_2NH_2]^{+}$cations, although the supercell expansion within the *ab* plane is also required for the reorientation of neighbouring ErO_8 polyhedra by approximately 180° along the two axes where the polyhedra are connected by a mixture of formate and oxalate ligands. The supercell of $[(NH_2)_3C]Er(HCO_2)_2(C_2O_4)$ allows similar alternating orientation of the $[(NH_2)_3C]^{+}$ cations and ErO_8 poly-

hedra within the *ac* plane, although the $2\sqrt{2}$ expansion of the *c*-axis seems to be primarily required by alternating orientations of both types of ligands along this direction.

There are bifurcated hydrogen bonds between each hydrogen in the NH_2 group and an oxygen atom attached to each of a formate and oxalate ligand with donor–acceptor distances of between 2.987(6) and 3.088(6) Å at 293 K. There are more extensive, but longer, hydrogen bonds between the $[(NH_2)_3C]^+$ cations and the framework it is encased in, the two equivalent NH_2 groups are involved in one single and one bifurcated hydrogen bonds with oxygen atoms from one oxalate and two formate ligands with donor–acceptor distances of 3.068(15) and 3.127(15) Å. The third NH_2 group is involved with two bifurcated hydrogen bonds at distances of 3.119(18) and 3.228(9) Å with oxygen atoms from oxalate ligands.

In these materials both $[(CH_3)_2NH_2]^+$ and $[(NH_2)_3C]^+$ cations remain ordered up to 500 K, the highest temperature examined in this study, with no change in symmetry detected. While the extensive hydrogen bonding facilitated by the $[(NH_2)_3C]^+$ cations enables ordering in these above ambient temperature in the $[(NH_2)_3C]M(HCO_2)_3$ (M = a divalent transition metal or magnesium cation),[27,28] this is well above the ordering temperature of the $[(CH_2)_2NH_2]M(HCO_2)_3$, which only order below ambient temperature, with the exception of the Jahn–Teller distorted Cu phase.[29–32] The increase in the strength of the hydrogen bonding may arise from (a) the substitution of the oxalate ligand for the formate linker and/or (b) the greater polarisation of the Er–O bonds, caused by the low electronegativity of the lanthanides, which increases the charge on the oxygen atoms of the ligand and thus stronger hydrogen bonds with the A-site cation. Regardless of its origins, the retention of A-site cation order to high temperature in these materials is significant with respect to the potential for related compounds to be ferroelectric at ambient temperatures. Although the materials reported here are centrosymmetric, we expect exchanging these A-site cations for those with different shape and hydrogen bond directionality will lead to compounds with polar ordering patterns, as is well established for the $AM(HCO_2)_3$ phases.

The thermal expansion of $[(NH_2)_3C]Er(HCO_2)_2(C_2O_4)$, analysed from 100–500 K using the program PASCal,[33] indicates the *c*-axis undergoes NTE of $-33.7(8)$ MK^{-1} with the *a*-axis and *b*-axis undergoing positive thermal expansion (PTE) of 57.7(8) and 11.4(7) MK^{-1}, respectively, leading to PTE of the unit cell volume of 35.9(1.7) MK^{-1} overall (see Fig. 2 for lattice parameters). The thermal expansion of $[(NH_2)_3C]Er(HCO_2)_2(C_2O_4)$ is consistent with behaviour seen in the anisotropic NTE and zero linear compressibility of the orthorhombic $[(NH_2)_3C]M(HCO_2)_3$ (M = Mn or Co) phases, which also occur along the *c*-axis, which is parallel to the plane of every $[(NH_2)_3C]$ cation.[34,35] In the $[(NH_2)_3C]M(HCO_2)_3$ phases, the observed anisotropic thermal expansion has been rationalised in terms of hinging of the metal–formate framework, which is also observed for $[(NH_2)_3C]Er(HCO_2)_2(C_2O_4)$ within the *ac*-plane (Fig. 1b and Fig. S5a†). Framework hinging combines with expansion of M–formate–M struts upon heating to give

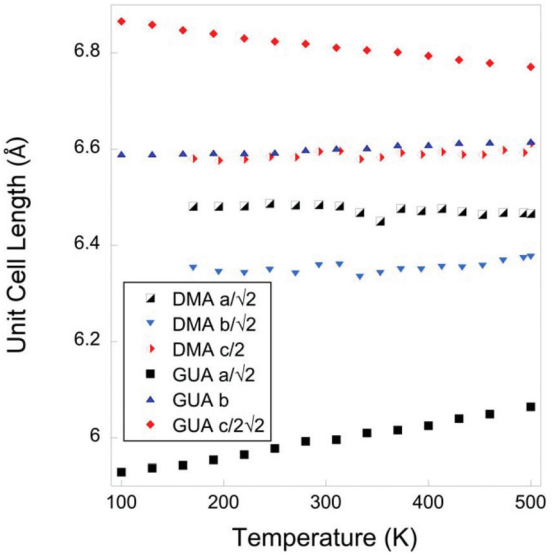

Fig. 2 Plot of unit cell lengths *versus* temperature for $[(CH_3)_2NH_2]Er(HCO_2)_2(C_2O_4)$ and $[(NH_2)_3C]Er(HCO_2)_2(C_2O_4)$ determined using single crystal X-ray diffraction. Errors in lattice parameters are smaller than the symbols. β angles fluctuate between 96.643(14)–97.185(2)° with temperature for $[(CH_3)_2NH_2]Er(HCO_2)_2(C_2O_4)$.

the overall observed thermal expansivities.[32,34] As is also seen here, this leads to greater expansion of the *a*-axis ($PTE_{hinging}$ + PTE_{strut}) which is accompanied by a more modest contraction along the *c*-axis ($NTE_{hinging}$ + PTE_{strut}), and finally a small expansion along the *b*-axis solely from strut expansion.

The direction along which the large PTE and NTE occurs in $[(NH_2)_3C]Er(HCO_2)_2(C_2O_4)$ can be rationalised from the angles between the Er cations within the *ac* plane. Hinging of the framework will tend towards a more isotropic pore shape to accommodate the guanidinium cation.[34] Thus the angles between connected Er^{3+} coordination along the *a*-axis of 98° and those of 78°/86° along the *c*-axis (at 100 K) will decrease and increase, respectively, leading to the observed large PTE along the *a*-axis and NTE along the *c*-axis (Fig. S3a†). Interestingly hinging induced thermal expansion in $[(NH_2)_3C]Er(HCO_2)_2(C_2O_4)$ appears more extreme than in the $[(NH_2)_3C]M(HCO_2)_3$ phases.[34] Thus $[(CH_3)_2NH_2]Er(HCO_2)_2(C_2O_4)$ will likely exhibit zero or negative linear compressibility along the *c*-axis under pressure.[35]

The thermal expansion along the principal axes (the orthogonal axes along which thermal expansion occurs purely in a linear fashion)[33] of monoclinic $[(CH_3)_2NH_2]Er(HCO_2)_2(C_2O_4)$ are much more modest. Using the program PASCal,[33] the expansivities were calculated at 10(3), 12(3) and $-8.9(1.6)$ MK^{-1} for the ⟨0,1,0⟩, ⟨−0.673,0,−0.740⟩ and ⟨−0.934,0,0.359⟩ directions, respectively, from 170 K to 500 K (see Fig. 2 for lattice parameters and Fig. S6† for orientation of the principal axes compared to the framework pore). $[(CH_3)_2NH_2]Er(HCO_2)_2(C_2O_4)$ is more rigid than both the $[(NH_2)_3C]$ analogue and the $[(CH_3)_2NH_2]M(HCO_2)_3$ family.[34] Framework hinging is greatly reduced compared to those

materials as can be seen from the evolution of the Er connected framework angles (Fig. S5b†). Only one framework angle varies noticeably with heating, which corresponds to the part of the framework where there are no hydrogen bonding interactions from the DMA cation. This suggests that the stronger hydrogen bonding that leads to the $[(CH_3)_2NH_2]^+$ cations retaining order in $[(CH_3)_2NH_2]Er(HCO_2)_2(C_2O_4)$ to 500 K is also responsible for greater rigidity in the framework, compared to the $[(CH_3)_2NH_2]M(HCO_2)_3$ family. The effect of hydrogen bonding strength on mechanical properties was also noted for $[C(NH_2)_3]Mn(HCO_2)_3$ and $[(CH_2)_3NH_2]Mn(HCO_2)_3$.[36]

Samples of both phases were confirmed to have high bulk purity using powder X-ray diffraction (see ESI† for experimental description and Fig. S7 and S8† for Le Bail fits to the data). This was confirmed by the Elemental Microanalysis Service at London Metropolitan University, which yielded 18.38% C, 2.56% H and 3.52% N for $[(CH_3)_2NH_2]Er(HCO_2)_2(C_2O_4)$ *cf.* 18.41% C, 2.58% H and 3.58% N while 15.15% C, 1.60% H and 10.23% N were obtained for $[(NH_2)_3C]Er(HCO_2)_2(C_2O_4)$ *cf.* to 14.81%, 1.99% H and 10.37% N. $[(CH_3)_2NH_2]Er(HCO_2)_2(C_2O_4)$ and $[(NH_2)_3C]Er(HCO_2)_2(C_2O_4)$ remain stable when heated in nitrogen to about 560 K and 650 K, respectively, above which they decompose endothermically (see ESI† for details of thermogravimetric analysis and Fig. S9 & S10† for plots of this data). $[(NH_2)_3C]Er(HCO_2)_2(C_2O_4)$ decomposes at significantly higher temperatures than related $ALn(HCO_2)_4$[20–22] or $[(NH_2)_3C]M(HCO_2)_3$ materials[27,28] and does not change significantly when the sample is heated under air (see Fig. S11†) indicating this is retained under oxidising conditions. The infrared spectra of the compounds are very similar with broad features around 3200–3500 cm^{-1} from N–H stretches and near 3000 cm^{-1} from C–H stretches, strong sharp features at about 1500–1600 and 800 cm^{-1} due to C–O modes, 1300–1450 cm^{-1} consistent with C–H bending modes and 1000–1100 cm^{-1} from C–N bends (see ESI, including Fig. S12,† for further details).

The radially contracted nature of Er's 4f electrons means any magnetic coupling in these materials is likely to be subtle and similar given the analogous coordination environments and connectivity of the B-site cations. We have measured the zero field cooled (ZFC) and field cooled (FC) magnetic susceptibility of $[(CH_3)_2NH_2]Er(HCO_2)_2(C_2O_4)$ under an applied field of 1000 Oe (see Fig. 3 for data, experimental details given in the ESI†). These remain paramagnetic down to 2 K, with a plot of the inverse ZFC susceptibility data well fitted by Curie–Weiss law down to 10 K, below which there is a small deviation, possibly due to crystal field effects quenching part of the orbital angular moment. This fit yields a Weiss temperature, Θ_W, of −6.4 K and an effective magnetic moment of 9.43μ_B *cf.* to 9.58μ_B calculated from Russell–Saunders equation. The Θ_W suggests that the magnetic coupling in the compound is antiferromagnetic, consistent with the significant decrease observed in $\chi_M T$ at temperature below 50 K (see Fig. S13†). Magnetisation measurements carried out at 2 K increase linearly up to 10 kOe before beginning to saturate at around 5μ_B per Er cation (see Fig. S14†). Consistent with paramagnetic behaviour there is no hysteresis observed.

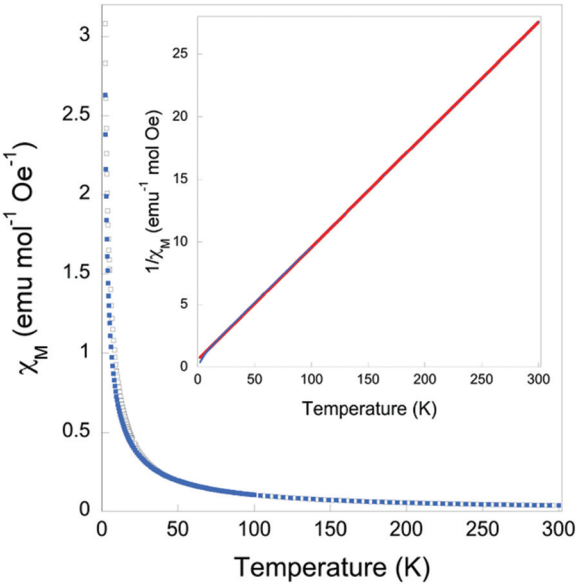

Fig. 3 Plot of χ *versus* temperature for $[(CH_3)_2NH_2]Er(HCO_2)_2(C_2O_4)$ for fields of 1000 Oe with ZFC and FC data shown as hollow black and filled blue markers, respectively. The insert shows a linear fit to the inverse FC susceptibility.

This work has reported the synthesis and crystal structures of $[(CH_3)_2NH_2]Er(HCO_2)_2(C_2O_4)$ and $[(NH_2)_3C]Er(HCO_2)_2(C_2O_4)$, the first hybrid ABX_3 perovskites with a combination of monovalent and divalent ligands. While these materials are centrosymmetric their A-site cations remain ordered to 500 K, suggesting modification of the A-site cation in these materials to those adopting a polar ordering pattern may lead to phases with interesting piezoelectric and ferroelectric properties at ambient temperature. We also observe anisotropic NTE in $[(NH_2)_3C]Er(HCO_2)_2(C_2O_4)$, which can be rationalised *via* a similar mechanism as used for the related $[(NH_2)_3C]M(HCO_2)_3$ phases but with a greater magnitude than reported in these materials. $[(CH_3)_2NH_2]Er(HCO_2)_2(C_2O_4)$ is shown to have a greater rigidity and have weak antiferromagnetic coupling.

Conflicts of interest

There are no conflicts to declare.

Acknowledgements

We would like to thank EPSRC for funding *via* project EP/R011524/1. LGB, JHBL and AKS completed the investigation including synthesis and data analysis. IEC rationalised the observed thermal expansion behaviour. PJS supervised the project team and conceptualised the study. PJS drafted the manuscript with all authors contributing to this. There are no conflicts to declare.

References

1 J. B. Goodenough, *Rep. Prog. Phys.*, 2004, **67**, 1915–1993.
2 B. Raveau, A. Maignan, C. Martin and M. Hervieu, *Chem. Mater.*, 1998, **10**, 2641–2652.
3 C. Moure and O. Peña, *Prog. Solid State Chem.*, 2015, **43**, 123–148.
4 M. Kubicek, A. H. Bork and J. L. M. Rupp, *J. Mater. Chem. A*, 2017, **5**, 11983–12000.
5 R. H. Mitchell, *Perovskites: Modern and Ancient*, Almaz Press, Thunder Bay, Ontario, 2002.
6 S. D. Stranks and H. J. Snaith, *Nat. Nanotechnol.*, 2015, **10**, 391–402.
7 B. Saparov and D. B. Mitzi, *Chem. Rev.*, 2016, **116**, 4558–4596.
8 H. S. Jung and N.-G. Park, *Small*, 2015, **11**, 10–25.
9 W. Li, Z. Wang, F. Deschler, S. Gao, R. H. Friend and A. K. Cheetham, *Nat. Rev. Mater.*, 2017, **2**, 16099.
10 Z. Wang, K. Hu, S. Gao and H. Kobayashi, *Adv. Mater.*, 2010, **22**, 1526–1533.
11 G. Rogez, N. Viart and M. Drillon, *Angew. Chem., Int. Ed.*, 2010, **49**, 1921–1923.
12 W.-J. Xu, S. Kopyl, A. Kholkin and J. Rocha, *Coord. Chem. Rev.*, 2019, **387**, 398–414.
13 Y. Wu, T. Binford, J. A. Hill, S. Shaker, J. Wang and A. K. Cheetham, *Chem. Commun.*, 2018, **54**, 3751–3754.
14 X.-H. Zhao, X.-C. Huang, S.-L. Zhang, D. Shao, H.-Y. Wei and X.-Y. Wang, *J. Am. Chem. Soc.*, 2013, **135**, 16006–16009.
15 L. C. Gómez-Aguirre, B. Pato-Doldán, A. Stroppa, L.-M. Yang, T. Frauenheim, J. Mira, S. Yáñez-Vilar, R. Artiaga, S. Castro-García, M. Sánchez-Andújar and M. A. Señarís-Rodríguez, *Chem. – Eur. J.*, 2016, **22**, 7863–7870.
16 S. M. Bovill and P. J. Saines, *CrystEngComm*, 2015, **17**, 8319–8326.
17 A. Cornia, A. Caneschi, P. Dapporto, A. C. Fabretti, D. Gatteschi, W. Malavasi, C. Sangregorio and R. Sessoli, *Angew. Chem., Int. Ed.*, 1999, **38**, 1780–1782.
18 Y.-Q. Tian, Y.-M. Zhao, H.-J. Xu and C.-Y. Chi, *Inorg. Chem.*, 2007, **46**, 1612–1616.
19 P. Samarasekere, X. Wang, W. Kaveevivitchai and A. J. Jacobson, *Cryst. Growth Des.*, 2015, **15**, 1119–1128.
20 A. Rossin, G. Giambastiani, M. Peruzzini and R. Sessoli, *Inorg. Chem.*, 2012, **51**, 6962–6968.
21 B. Liu, H.-B. Zheng, Z.-M. Wang and S. Gao, *CrystEngComm*, 2011, **13**, 5285–5288.
22 T.-M. Zhao, S. Chen, R. Shang, B.-W. Wang, Z.-M. Wang and S. Gao, *Inorg. Chem.*, 2016, **55**, 10075–10082.
23 W. Yao, Y.-Y. Guo and P. Lightfoot, *Dalton Trans.*, 2017, **46**, 13349–13351.
24 R. Clulow, A. J. Bradford, S. L. Lee and P. Lightfoot, *Dalton Trans.*, 2019, **48**, 14461–14466.
25 X. He, X. Zhang, B. Ji, W. Yao, P. Lightfoot and Y. Tang, *Chem. Commun.*, 2021, **57**, 2567–2570.
26 A. Trzesowska, R. Kruszynski and T. J. Bartczak, *Acta Crystallogr., Sect. B: Struct. Crystallogr. Cryst. Chem.*, 2004, **60**, 174–178.
27 K.-L. Hu, M. Kurmoo, Z. Wang and S. Gao, *Chem. – Eur. J.*, 2009, **15**, 12050–12064.
28 A. Rossin, M. R. Chierotti, G. Giambastiani, R. Gobetto and M. Peruzzini, *CrystEngComm*, 2012, **14**, 4454–4460.
29 P. Jain, V. Ramachandran, R. J. Clark, H. D. Zhou, B. H. Toby, N. S. Dalal, H. W. Kroto and A. K. Cheetham, *J. Am. Chem. Soc.*, 2009, **131**, 13625–13627.
30 T. Asaji, S. Yoshitake, Y. Ito and H. Fujimori, *J. Mol. Struct.*, 2014, **1076**, 719–723.
31 P. Jain, N. S. Dalal, B. H. Toby, H. W. Kroto and A. K. Cheetham, *J. Am. Chem. Soc.*, 2008, **130**, 10450–10451.
32 I. E. Collings, M. Bykov, E. Bykova, M. Hanfland, S. van Smaalen, L. Dubrovinsky and N. Dubrovinskaia, *CrystEngComm*, 2018, **20**, 3512–3521.
33 M. J. Cliffe and A. L. Goodwin, *J. Appl. Crystallogr.*, 2012, **45**, 1321–1329.
34 I. E. Collings, J. A. Hill, A. B. Cairns, R. I. Cooper, A. L. Thompson, J. E. Parker, C. C. Tang and A. L. Goodwin, *Dalton Trans.*, 2016, **45**, 4169–4178.
35 Z. Yang, G. Cai, C. L. Bull, M. G. Tucker, M. T. Dove, A. Friedrich and A. E. Phillips, *Philos. Trans. R. Soc., A*, 2019, **377**, 20180227.
36 W. Li, A. Thirumurugan, P. T. Barton, Z. Lin, S. Henke, H. H.-M. Yeung, M. T. Wharmby, E. G. Bithell, C. J. Howard and A. K. Cheetham, *J. Am. Chem. Soc.*, 2014, **136**, 7801–7804.